Radio-frequency sputtering fabrication of chalcogenide-based Er3+-doped vertical optical cavities for near-infrared operation

Simone Normani, Jan Gutwirth, Loïc Bodiou, Marion Baillieul, Loïc Joanny, Joël Charrier, Petr Nemec, Virginie Nazabal

Research Article | Vol. 10, No. 10 / 1 October 2020 / Optical Materials Express 2500
Optical Materials EXPRESS

Radio-frequency sputtering fabrication of chalcogenide-based Er^{3+}-doped vertical optical cavities for near-infrared operation

Simone Normani,[1] Jan Gutwirth,[1] Loïc Bodiou,[3] Marion Baillieul,[1] Loïc Joanny,[2] Joel Charrier,[3] Petr Němec,[1] and Virginie Nazabal[1,2,*]

[1]Department of Graphic Arts and Photophysics, Faculty of Chemical Technology, University of Pardubice, 53210 Pardubice, Czech Republic
[2]Univ Rennes, CNRS, ISCR (Institut des Sciences Chimiques de Rennes) – UMR 6226, F-35000 Rennes, France
[3]Univ Rennes, CNRS, Institut FOTON - UMR 6082, F-22305 Lannion, France
*virginie.nazabal@univ-rennes1.fr

Abstract: Chalcogenide-oxide Bragg reflectors and a 1-D vertical cavity for operation at 1.55 µm were designed and fabricated *via* radio-frequency sputtering. The Bragg reflectors were made out of repeating layers of Al_2O_3 and As_2Se_3, and the cavity was obtained *via* a $Ga_5Ge_{20}Sb_{10}S_{65}$:Er^{3+} defect layer. The layers' properties were assessed via ellipsometry and SEM imaging. Transmission spectroscopy verifies the appearance of a well-defined stop-band centered around 1.5 µm with a very wide bandgap, and extremely low transmission, even with a relatively low layer count. The vertical optical cavity fabrication results in the appearance of a resonance within the band, at a wavelength corresponding to the $^4I_{13/2} \rightarrow {}^4I_{15/2}$ transition of erbium. The high transmittance at 808 and 980 nm allows for optical pumping, and thus light amplification and coherent light generation from the cavity. The operation of these devices was investigated, showing coherent light emission at 1.5 µm. The results are encouraging in assessing the viability of this design and these materials for operation in the near-infrared range, providing an important step towards the fabrication of chalcogenide-based optical amplifiers for the near-infrared.

1. Introduction

In recent years, optical materials and devices for operation in the infrared range have been a point of strong interest for research, due to the many interesting potential uses they provide, ranging from medical applications to astrophysics [1–4]. In this context, chalcogenide glasses have gained great popularity, owing to their wide transparency range and high refractive index in the near-infared (NIR) and mid-infrared (MIR) [5–7]. The development of IR light sources and amplifiers is therefore an important part of this field: in particular, compact sources and integrated devices make for very interesting research topics. Light amplification and laser generation can be obtained through high-quality factor optical cavities fabricated with the use of interferential mirrors [8–10], which can be obtained by RF-sputtering [11,12]. In literature, optical cavities and micro-resonators for operation in the NIR range have been successfully obtained with the use of common oxide glasses, semiconductors, and polymers [13–15], however, there is not much information about similar chalcogenide-based structures doped with rare earth, which could provide a key step towards the subsequent development of devices for application at longer wavelengths. It is noteworthy that Bragg reflectors (BRs) as infrared interferential filters have been successfully fabricated using chalcogenide glasses by electron beam-assisted evaporation [16]. The interest of using chalcogenides as main materials is not only that of extending the application

#401930 https://doi.org/10.1364/OME.401930
Journal © 2020 Received 7 Jul 2020; revised 22 Aug 2020; accepted 22 Aug 2020; published 15 Sep 2020

Optical Materials EXPRESS

of multilayer structures and active resonators further into the MIR range with ever-improving efficiency, but they provide interesting application in non-linear optics which can be employed for a large variety of applications [17–19]. Amorphous chalcogenides thin films were used as a photosensitive material [20–25] for spacer and high refractive index material of narrow band-pass filters to allow post-trimming of these devices using a light beam. The objective was not only to correct the consequences of deposition errors on the filter properties with precision, but also to create entirely new filter devices with controlled spatial properties, e.g., variable filters with arbitrary profile or an anodizing filter with spatially structured transmittance/reflectance response [26,27]. Moreover, previous efforts have yielded encouraging results in obtaining Er^{3+} doped chalcogenide-based optical cavities, depositing the multilayer structures via laser ablation [28]. Chalcogenide-based photonic crystals and optical cavities are therefore an extremely appealing set of devices, as they can be implemented as free-standing elements as well as integrated components in waveguides and fiber optics [20,29].

Consequently, in this work, chalcogenide-based devices for operation in the infrared are designed, fabricated and characterized, showing their optical properties and the viability of their design, and intending to lead further on to the development of optical amplifiers and laser sources in deeper MIR regions.

2. Materials and methods

In order to fabricate performant optical cavities in the near-to-mid infrared, it is first and foremost essential to obtain the appropriate distributed BRs. The choice of materials must take into account the transparency in the desired spectral range and the difference in refractive index between the different layers, since a larger refractive index contrast provides higher reflectivity and wider stop-bands. For this purpose, Al_2O_3 and As_2Se_3 were chosen as the low- and high-refractive index materials respectively, because they have a refractive index difference greater than 1 across the range of interest, and high transparency in the NIR. The $Ga_5Ge_{20}Sb_{10}S_{65}$:Er^{3+} glass was chosen as the defect material, as it possesses favorable optical qualities such as high transmission over a very broad region from NIR to MIR, and provides a good solubility for rare earths [30,31]; erbium in particular was chosen as dopant for its well-known transitions and common use in active devices and coherent light sources.

Three two-inch sputtering targets, Al_2O_3 (ALB Materials), As_2Se_3 (VITRON), and $Ga_5Ge_{20}Sb_{10}S_{65}$:Er^{3+} (fabricated by melt-quenching technique [16,31]) with 10^4 ppm doping concentration were installed in a radio-frequency co-sputtering cathode cluster within a vacuum chamber, so that each layer could be deposited independently without changing the substrate position. The depositions were performed under 0.5 Pa argon pressure, with a 75 sccm argon flow, and keeping a steady 5 rpm rotation of the substrate holder. The applied power for the three cathodes was 150 W for Al_2O_3, 15 W for As_2Se_3, and 20 W for $Ga_5Ge_{20}Sb_{10}S_{65}$:Er^{3+}.

Several depositions on silicon wafer substrates were performed for each material at different distances between cathodes, ranging from 5 cm to 8.5 cm; the optimal distance was identified by trade-off of deposition rates for layer thickness homogeneity. These values were obtained via variable angle spectroscopic ellipsometry (VASE) in the UV-to-NIR range.

Both a 10-layer BR and a 20-layer BR were deposited on 1-inch glass (BK7) substrates placed at the center of the substrate holder. A silicon substrate was also placed on the holder in order to have a sample for ellipsometry measurements. The BRs were deposited alternating Al_2O_3 and As_2Se_3 layers. The deposition time for the layers was estimated using the values of refractive index and deposition rate, to have for each of them an optical thickness equal to $\lambda_R/4$ for the resonance wavelength λ_R of 1.55 µm, corresponding to the main NIR emission of Er^{3+}. The deposition began with the low-index material, Al_2O_3, for a softer index transition from the BK7 substrate to the BR, thus reducing Fresnel losses.

Optical Materials EXPRESS

VASE measurements were performed with a J. A. Woollam ellipsometer on the control samples deposited on the silicon substrate so as to check refractive index and thickness of the BR layers. The measurements were taken in the 300–2300 nm range with a 5 nm step and averaging over 30 revolutions at each wavelength.

Scanning Electron Microscope (SEM) images of the cross-section of the multilayers were recorded using a JEOL JSM 7100 F instrument. To record these images, the BRs samples, deposited on a silicon substrate, were cleaved at a position that was close to the substrate holder center during deposition.

Fluorescence measurements were performed on the vertical cavity by mounting the sample on a holder, exciting the film at 980 nm and collecting the near-field signal through a multimode fiber leading to a near-infrared spectrometer (Oceanoptics NIRQuest). A commercial 980 nm laser diode driven by a temperature and current controller (ILX Lightwave LDC 3742) was used to obtain the pump beam, which was carried through a fiber and focused with a lens of 25.4 mm focal length onto the sample through the substrate, collecting the signal on the other side.

Transmission spectroscopy was performed on the BRs deposited on BK7 substrates with a Perkin-Elmer spectrometer to assess reflectivity and stop-band width around λ_R. The measurement was performed with a 1 nm monochromator bandwidth and using a circular diaphragm with 5 mm diameter to limit the beam size to the center of the sample.

Reflection spectroscopy measurements were also performed, using the Woollam ellipsometer, at an angle of 30° from the normal to the surface. While this causes a shift in the position of the spectral features of the device, it nonetheless allows an approximate representation of the optical and spectroscopic properties for the BRs.

3. Results and discussion

The results of the single film thickness estimate from VASE are shown in Fig. 1. The maximum thickness of the film was 400 ± 1 nm for As_2Se_3, 244 ± 1 nm for Al_2O_3, and 352 ± 1 nm for $Ga_5Ge_{20}Sb_{10}S_{65}$:Er^{3+}, obtained at a 5 cm target-to-substrate distance. The ellipsometry measurements also provided the actual refractive index dispersion curves for all three materials, and most importantly an accurate value for their refractive index at the operating wavelength of 1550 nm, that is to say 1.64 ± 0.01 for Al_2O_3, 2.77 ± 0.01 for As_2Se_3, and 2.24 ± 0.01 for $Ga_5Ge_{20}Sb_{10}S_{65}$:Er^{3+}. These values were then used in combination with the deposition rate estimates to adjust the deposition parameters for the device fabrication process.

As foreseen, the deposition rate is greater when the target-to-substrate distance is shorter, however there does not seem to be any obvious difference in the thickness homogeneity across depositions at different distances. Based on these results, the distance of 5 cm was deemed appropriate for further depositions. It is worth noting that the drop in layer thickness up to 1 cm distance from the film center is about 1% (Fig. 1), which allows us to consider the layers uniform across most of the surface of one-inch glass substrates that will be used for the final device.

The deposited 10-layer BR and a 20-layer BR samples are shown in Fig. 2. The absence of visible interference fringes suggests that the layers are rather uniform in thickness.

The SEM images of the BR cross-sections are shown in Fig. 3. The approximate estimate of the thickness for the different layers is consistent with expectations for both samples: both VASE and SEM imaging show a roughly 10% decrease in the thicknesses of all layers deposited on silicon with respect to the intended layer thickness values, which is expected due to the off-center position of the silicon substrates during deposition.

The thickness and refractive index of the different layers were estimated by fitting the ellipsometry data using the Cauchy model. The refractive index was considered equal across all layers of the same material in the fitting. It should be pointed out that the reliability of ellipsometry data fitting is somewhat lower in comparison with single thin films due to large number of layers. The 10-layer BR fit yielded on average 230 nm thick Al_2O_3 layers with a

Optical Materials EXPRESS

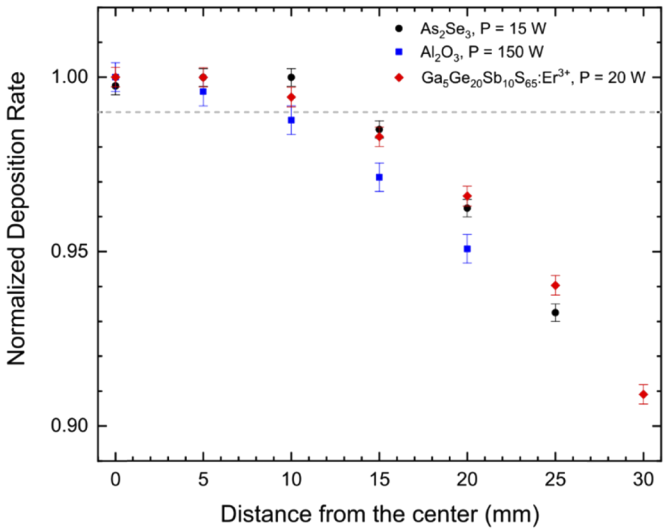

Fig. 1. Normalized sputtering deposition rate (estimated via VASE) for the various materials versus the distance from the center of the substrate showing the homogeneity of the layers around the center. The grey dashed line marks the 1% thickness drop.

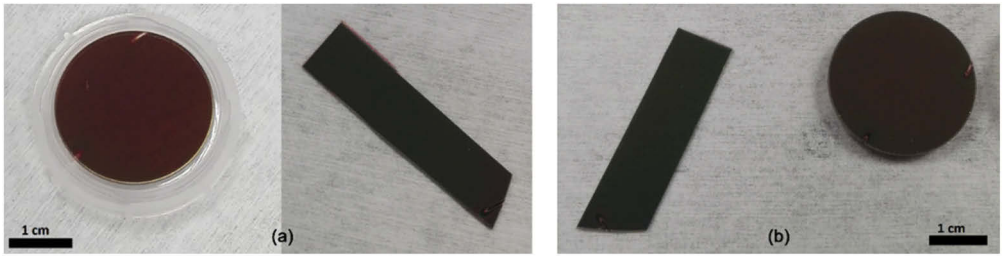

Fig. 2. (a) 5 + 5 layers BRs and (b) 10 + 10 layers BRs deposited on both BK7 substrates and silicon wafers.

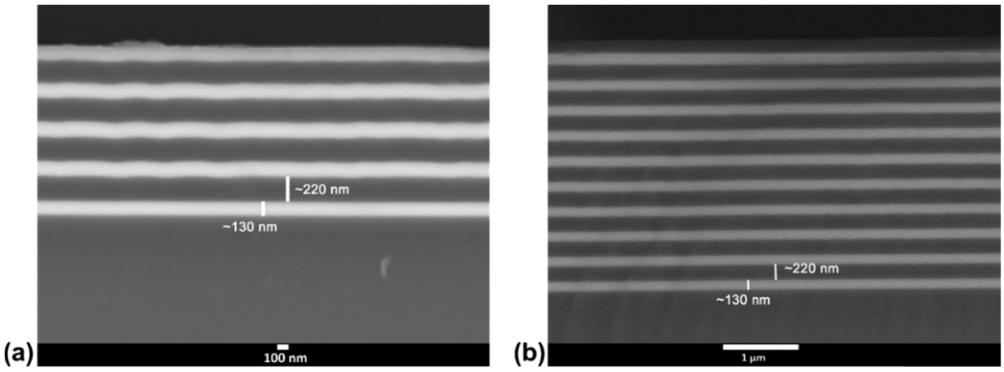

Fig. 3. SEM images of the multilayer BRs deposited on silicon substrates: (a) 10-layer BR, and (d) 20-layer BR. The pictures show the polished cleaved sections.

Optical Materials EXPRESS

refractive index of 1.64 ± 0.01 at 1.55 µm, and 130 nm thick As_2Se_3 layers with a refractive index of 2.81 ± 0.01 at 1.55 µm. The 20-layer BR fit yielded on average 230 nm thick Al_2O_3 layers with a refractive index of 1.67 ± 0.01 at 1.55 µm, and 130 nm thick As_2Se_3 layers with a refractive index of 2.79 ± 0.01 at 1.55 µm. The thickness average estimates have an uncertainty of 5 nm due to fluctuations between different layers, and the refractive index average estimates have an error of 2% at maximum. The thickness estimates are consistent with values indicated by SEM images (Fig. 3). One can notice some imperfections in interface homogeneity that carry over across the stacked layers at some spots. These small imperfections or layer oscillations can be also amplified by charge effects in SEM images. However, local imperfections do not seem to affect the overall integrity of the structure and do not entail any sensible issue in the spectroscopy.

The reflection spectroscopy measurements on the BRs, reported in Fig. 4, show that the deposition was successful in producing devices with a stop-band centered at the 1.55 µm wavelength. In particular, one can see that the more defined stop-band of the 20-layer BR is rather broad, having a width of 560 nm, but narrower than that of the 10-layer BR, which is about 690 nm wide. However, the 20-layer BR reflection around the 1.55 µm wavelength is sensibly enhanced, as it corresponds to a significant improvement with respect to the 10-layer BR, as the latter has a transmittance value of 0.13% at the resonant frequency, and the former has 0.001%. The reduction in stop-band width is not a crucial factor for the operation of the device, while the increase in reflectance is a very significant improvement, as it is the parameter, which will determine the quality factor of the cavity.

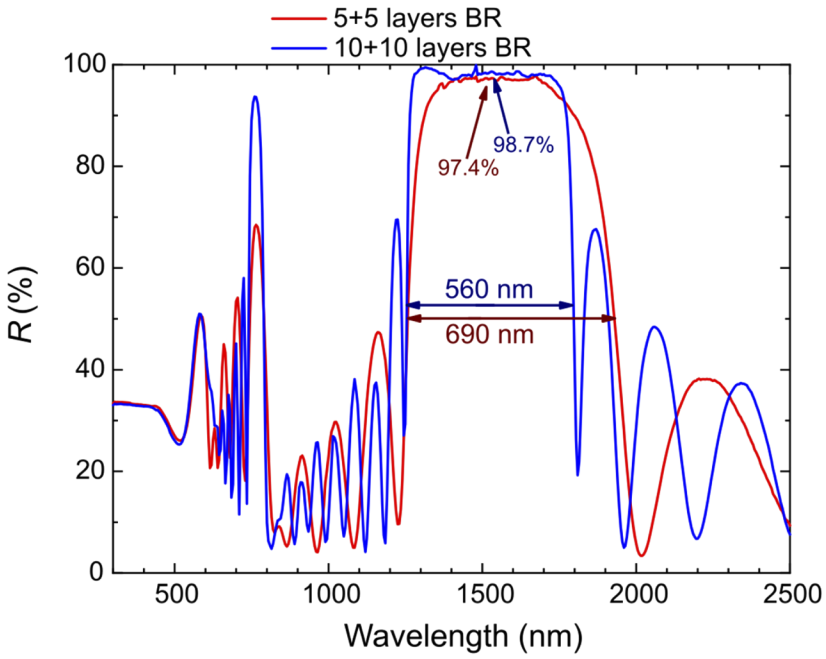

Fig. 4. Reflectivity spectra for the 10- and 20-layer BRs collected at a 30° incidence angle, showing the difference in stop-band shape, width and depth. The percentages at the top of the band show the reflectance values of the two BRs at 1.55 µm.

In addition, the reflection data were used in conjunction with transmission data to obtain an estimate of the reflectors absorbance. The absorbance A of the BRs were then calculated via the equation:

$$A = \log_{10}\left(\frac{1 - R^2}{T}\right) \tag{1}$$

Optical Materials EXPRESS

where R and T are the reflectance and transmittance respectively. The total UV absorption, extending over 600 nm due to the As_2Se_3 layers is clearly visible in the spectra (Fig. 5). Significant absorption is also present through the stop-band interval, however, these values are subject to very high uncertainty through Eq. (1) because of the extremely low transmission in that range.

Once the BR properties were assessed, a 41-layer optical resonator was fabricated by depositing a defect layer with optical thickness equal to $\lambda_R/2$ between two mirrored 20-layer Al_2O_3-As_2Se_3 BRs, as shown in Fig. 6. For the resonator, a SiO_2 glass substrate was placed in the center of the holder instead of the BK7 because of the higher transparency of the former, so as to optimize the overall performance of the final device.

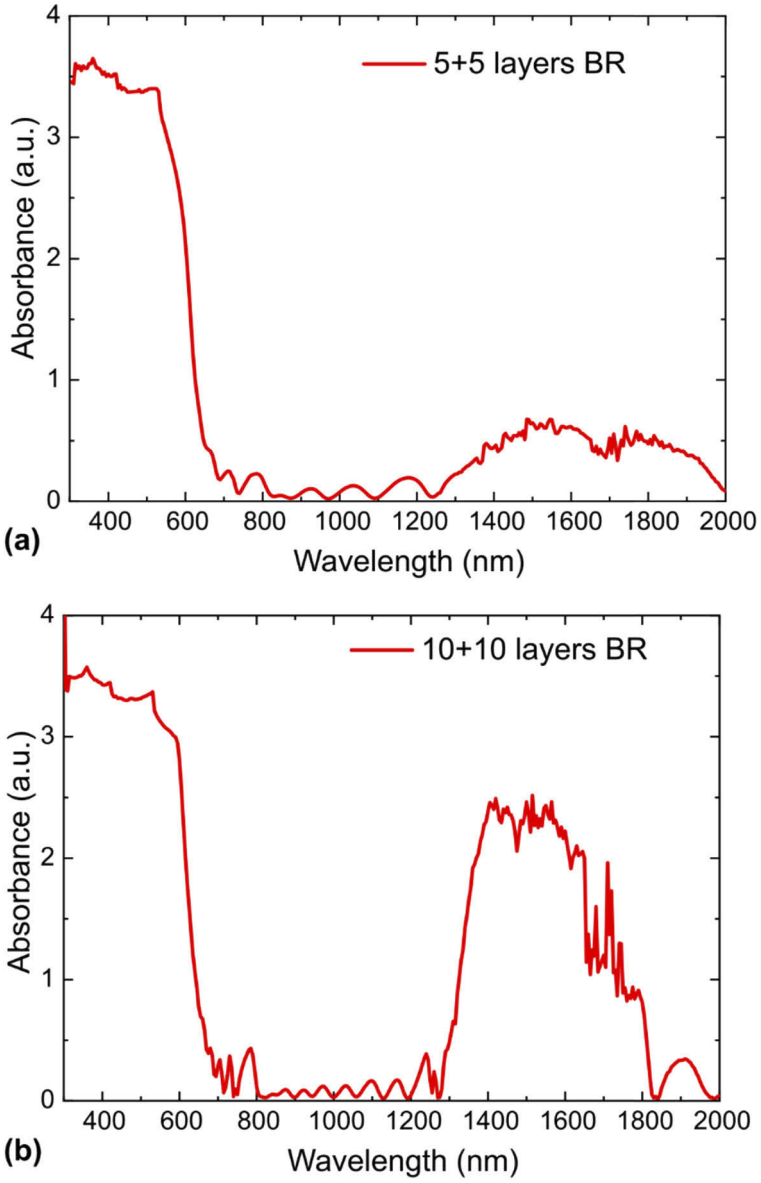

Fig. 5. Absorption spectra of the 10-layer (a) and 20-layer (b) BRs from the transmission and reflection data.

Optical Materials EXPRESS

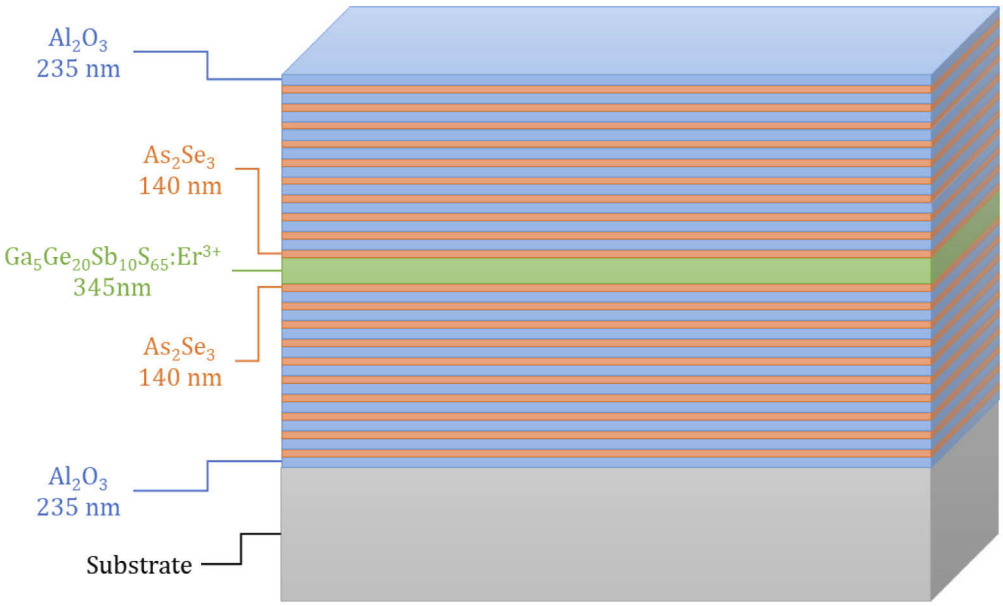

Fig. 6. Schematic representation of the $Ga_5Ge_{20}Sb_{10}S_{65}:Er^{3+}$ optical cavity enclosed between two 20-layer Al_2O_3-As_2Se_3 BRs.

Both transmission spectroscopy and VASE measurements were performed to assess the optical properties of the resonator. At the same time, a simulation for the spectroscopic properties of the device, based on the transfer-matrix formalism [32,33], was run in order to have a comparison between the experimental results and the theoretical expectations.

The optical transmission spectrum of the vertical cavity is shown in Fig. 7. Here, as expected due to the high number of BR layers, the optical stop-band is extremely well-defined and the transmission within it extremely low. One can nonetheless see the appearance of the transmission peak close to 1.5 µm, corresponding to the cavity resonance. Moreover, the transmission of the device is found as high as 94.3% at 808 nm and 84.1% at 980 nm, meaning losses of incident light at these wavelengths are low and the excitation of Er^{3+} ions is therefore theoretically efficient, which makes the device suitable for coherent light generation at 1.5 µm.

While the device resonance peak position is somewhat shifted from the Er^{3+} emission maximum wavelength (1550 nm), it still falls within the range of the $^4I_{13/2} \rightarrow {}^4I_{15/2}$ emission band, meaning operation with this system is still viable, although not as efficient. However, since considering a three-level laser system, this blue-shift entails that the light will incur in greater reabsorption from the ground state due to the relative increase in absorption cross-section with respect to the emission cross-section as per the McCumber relation [34], which is expected to reduce the total internal gain of the device. This shift is due to the uncertainty on the deposition rate estimates of the defect layer material, which caused the layer to be roughly 3% thinner than expected. One can see, in Fig. 7, the blue-shift in the experimental transmission spectrum with respect to the results of the simulation, which confirms the observation of the deposited BR layers and defect layer being generally thinner than expected.

The simulations allowed to obtain an estimate of the ideal-case cavity quality factor, which was calculated to be roughly $4.2 \cdot 10^4$ for a device with 20-layer BRs simply based on the transmission spectrum, while the actual quality factor was estimated of about 500, however this value is limited by the spectrophotometer resolution.

Optical Materials EXPRESS

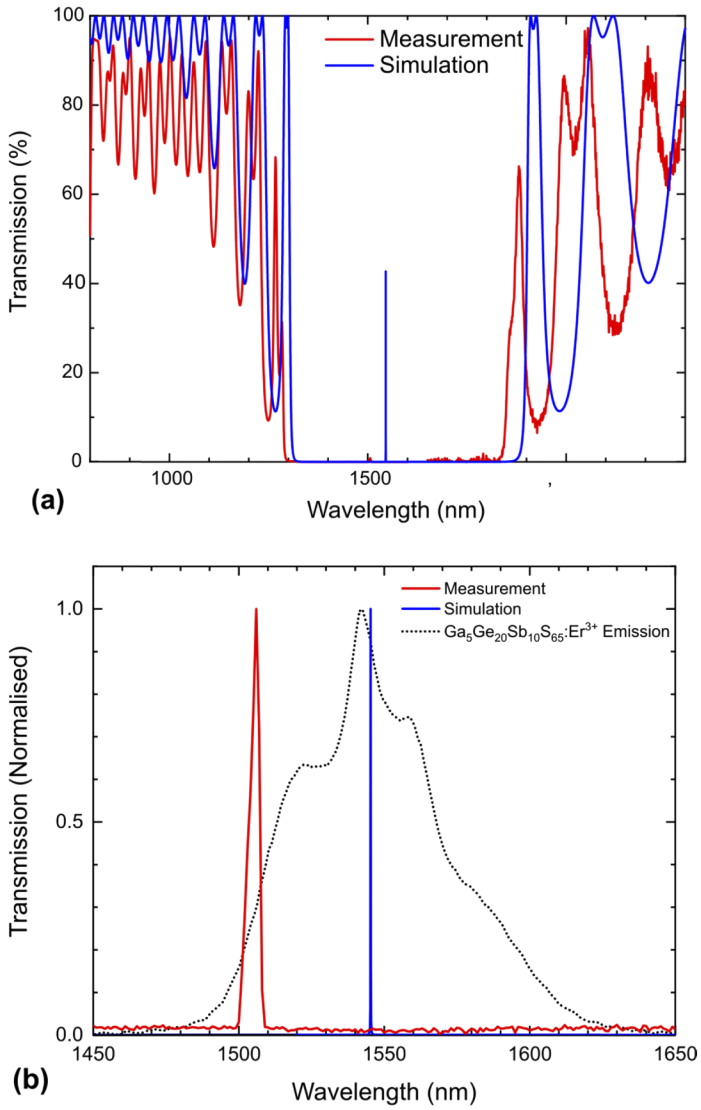

Fig. 7. (a) Comparison between the transmission measurements on the vertical cavity and the simulated spectrum obtained from the parameters used for designing the device, and (b) position of the resonance peaks compared with the $^4I_{13/2} \rightarrow {}^4I_{15/2}$ Er^{3+}emission band. The experimental single-layer parameters obtained from the initial deposition trials for each material were used in performing the simulations.

Fluorescence spectra however, show very little signal around 1.5 µm (Fig. 8). The emission peak appears over the noise as the pump power is increased, and rises monotonically with pump power. Nevertheless, the low intensity signals very strong quenching due to up-conversion of the pump power to the green Er^{3+} emission. The appearance and rise of a peak at the 1027 nm wavelength, corresponding to the second-order detection of 514 nm emission confirms that up-conversion takes place. This is an unfortunate side effect of the combination of relatively high Er^{3+} concentration with the BR third-order stop-band, centered very close to this particular wavelength corresponding to the $^2H_{11/2} \rightarrow {}^4I_{15/2}$ Er^{3+} emission. While this is deleterious to the

Optical Materials EXPRESS

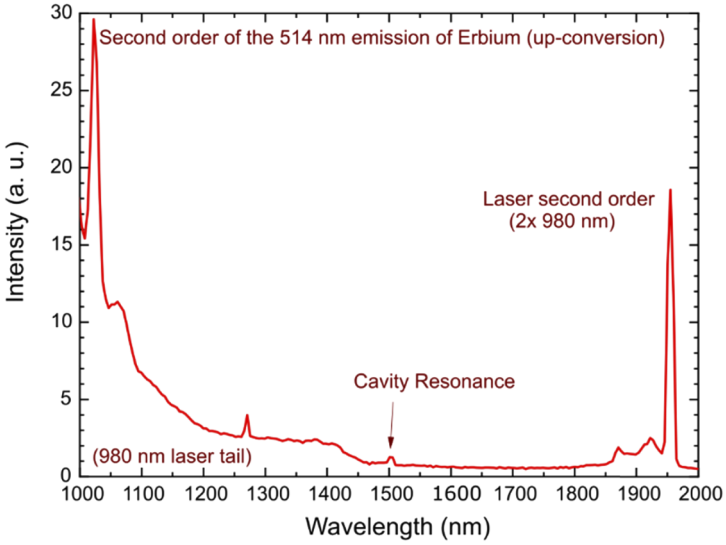

Fig. 8. Emission spectrum of a vertical cavity showing evidence of the generation of fluorescence in the green (appearance of the second order of the 514 nm emission) and infrared.

goal of obtaining an intense 1.5 µm emission, it is an encouraging result, as it attests the high degree of light confinement of the cavity, while the quenching issue can be addressed separately.

It is however possible to trace the 1.5 µm emission intensity as a function of the pump power. One can then notice (Fig. 9) the appearance of a clear threshold for this emission estimated around 5.2 mW, which, along with the narrow width of the visible peak, inferior to the instrument resolution, suggests the generation of coherent radiation. Interestingly, the data seem to deviate

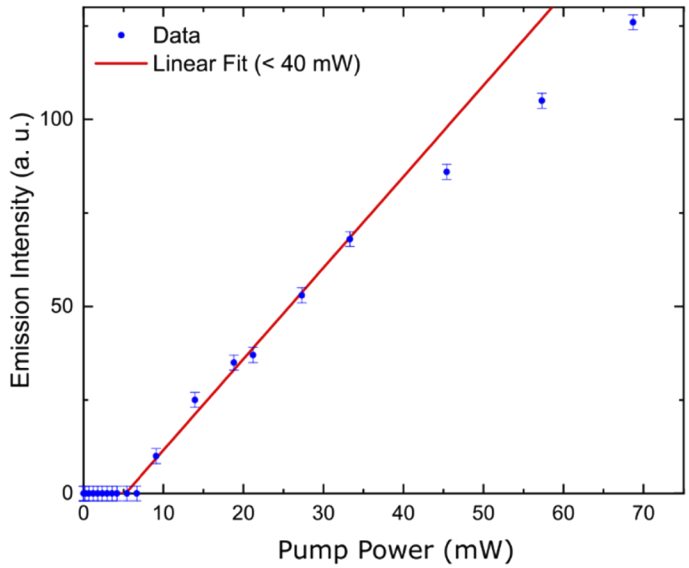

Fig. 9. Data and linear fit of the cavity emission at 1.5 µm, showing the estimated pump power.

Optical Materials EXPRESS

from the initial behavior at higher pump power, as the slope decreases indicatively above 40 mW. This is possibly indicative of nonlinear phenomena taking place in the cavity.

While the results of the fabrication were quite close to the expectations provided by the simulations, the emission spectroscopy clearly shows flaws in the final product that hinder the device efficiency. Keeping these observations in mind, some improvements can be considered

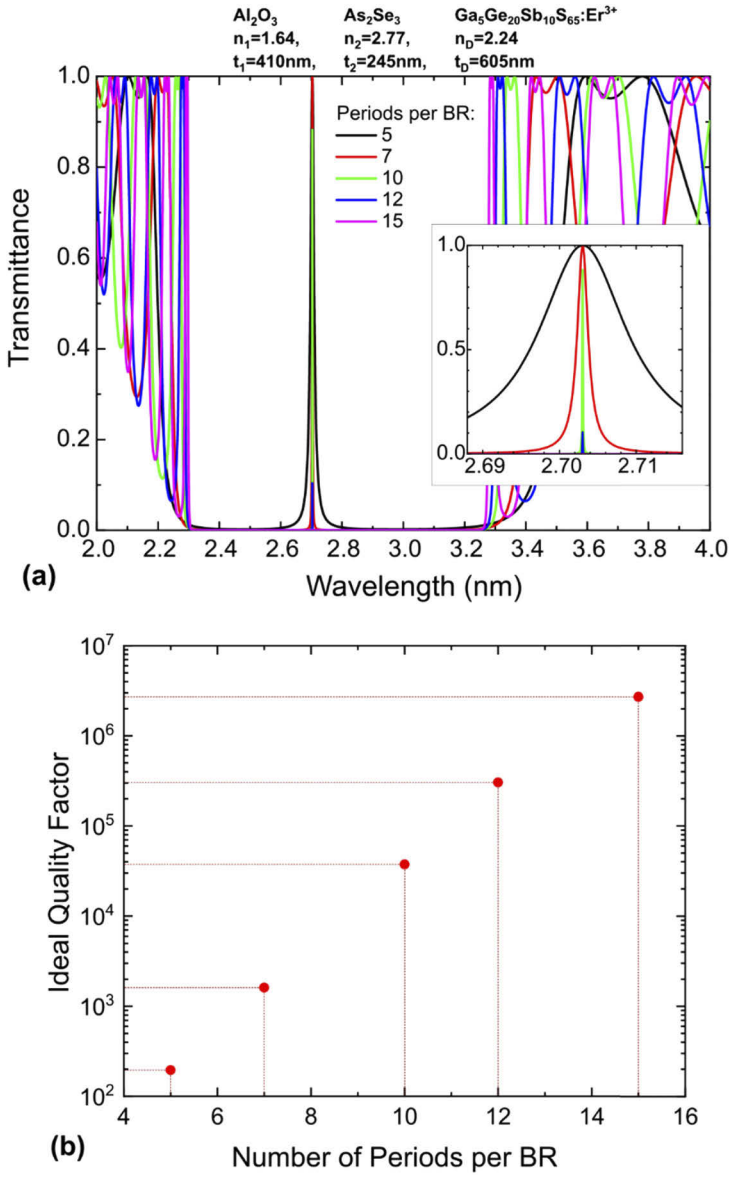

Fig. 10. (a) Transmission spectra of vertical cavities calculated via the transfer matrix formalism for operation within the $^4I_{11/2} \rightarrow {}^4I_{13/2}$ Er^{3+} emission band, showing the effect of different number of BR periods on the stop-band profile; (b) estimate of the ideal cavity quality factor as a function of the number of iterations of the BR layer pairs. This represents an ideal case in which absorption is zero, so actual cavity quality factors are expected to be sensibly lower.

Optical Materials EXPRESS

in order to obtain a more performant cavity. First of all, since the position of the resonance peak is crucial for the ratio of the emission/reabsorption cross-section, the optical properties of the device will be manipulated by subjecting it to thermal annealing, with the aim of possibly reducing the thin film porosity and improve its homogeneity, which will effectively increase the refractive index and therefore the optical length of the defect, and also via light exposure, to exploit the chalcogenides photosensitivity in order to better tailor the photonic bandgap and resonance. However for future trials, a better control of the optical thickness of the defect layer is needed. This can be achieved with more trials spent on fine-tuning the deposition parameters and time, or by installing a method of in-chamber detection of the deposited material, such as quartz microscales or an optical control. The other main issue is the high Er^{3+} doping concentration, which causes quenching of the $^4I_{13/2} \rightarrow {}^4I_{15/2}$ transition, and can be addressed by simply using a target with lower, better-suited rare earth ions concentration.

Since the simulations have shown to give a good approximation for the transmission and reflection spectra of 1DPCs, they can be used to perform a reasonable estimate of similar cavities for different wavelengths and emission lines. In particular, moving further into the Mid-IR, one can use these calculations to design an appropriate resonator for the $^4I_{11/2} \rightarrow {}^4I_{13/2}$ Er^{3+} emission at 2.7 µm. Figure 10 shows the results of the simulations for $Ga_5Ge_{20}Sb_{10}S_{65}$:Er^{3+} cavities with Al_2O_3-As_2Se_3 BRs. It is important to keep in mind, however, that the transmission values are higher than what can be expect from the actual device, as these simulations do not take into account absorption, which is even higher in the MIR than in the NIR for materials such as oxides, and the quality factor estimates present the ideal value, while the real one would be sensibly lower.

4. Conclusion

In the course of the work, Al_2O_3-As_2Se_3 distributed Bragg reflectors and a 1-D optical cavity with a $Ga_5Ge_{20}Sb_{10}S_{65}$:Er^{3+} defect layer were designed and deposited by radio-frequency sputtering. The layer thickness, uniformity and refractive index were estimated via SEM imaging and ellipsometry, and the devices were spectroscopically characterized. The spectroscopy shows encouraging results as the stop-band appears clearly around 1.5 µm with a relatively low number of layers: a total of 10 periods of alternating layers is sufficient to obtain a very well-defined stop-band with an almost zero transmittance at 1.55 µm. As expected, the addition of the defect layer causes the appearance of a transmission peak in the middle of the band, at a wavelength corresponding to the $^4I_{13/2} \rightarrow {}^4I_{15/2}$ transition of erbium, proving the viability of the material choice and design to obtain an efficient optical amplifier in the infrared. Further investigation is envisioned in order to extend the application of this design to the mid infrared, exploiting the wide infrared transparency window of chalcogenides to obtain similar resonators at 2.7 µm and possibly as far as 4.5 µm.

Funding

European Cooperation in Science and Technology (MP1401); Grantová agentura České republiky (19-24516S).

Acknowledgments

The project of International Mobility of Researchers at the University of Pardubice, OP RDE project CZ.02.2.69/0.0/0.0/16_027/0008008; the Czech Science Foundation (project No. 19-24516S); COST MP1401-STSM; Centre National de la Recherche Scientifique (CNRS); Brittany Region. Equipment funding of Institut Foton was partly provided by the CPER Sophie. Platform ScanMAT-CMEBA UMS CNRS 2001 at University of Rennes 1, FRANCE.

Optical Materials EXPRESS

Disclosures

The authors declare no competing interests.

References

1. M.-L. Anne, J. Keirsse, V. Nazabal, K. Hyodo, S. Inoue, C. Boussard-Pledel, H. Lhermite, J. Charrier, K. Yanakata, O. Loreal, J. Le Person, F. Colas, C. Compère, and B. Bureau, "Chalcogenide Glass Optical Waveguides for Infrared Biosensing," Sensors **9**(9), 7398–7411 (2009).
2. A. B. Seddon, "Mid-infrared (IR) - A hot topic: The potential for using mid-IR light for non-invasive early detection of skin cancer in vivo," Phys. Status Solidi B **250**(5), 1020–1027 (2013).
3. M. Le Corvec, F. Charpentier, A. Kachenoura, S. Bensaid, S. Henno, E. Bardou-Jacquet, B. Turlin, V. Monbet, L. Senhadji, O. Loréal, O. Sire, J. F. Betagne, H. Tariel, and F. Lainé, "Fast and Non-Invasive Medical Diagnostic Using Mid Infrared Sensor," IRBM **37**(2), 116–123 (2016).
4. H.-D. K. Goldsmith, N. Cvetojevic, M. Ireland, and S. Madden, "Fabrication tolerant chalcogenide mid-infrared multimode interference coupler design with applications for Bracewell nulling interferometry," Opt. Express **25**(4), 3038 (2017).
5. J. S. Sanghera, L. Brandon Shaw, and I. D. Aggarwal, "Chalcogenide Glass-Fiber-Based Mid-IR Sources and Applications," IEEE J. Sel. Top. Quantum Electron. **15**(1), 114–119 (2009).
6. B. J. Eggleton, B. Luther-Davies, and K. Richardson, "Chalcogenide photonics," Nat. Photonics **5**(3), 141–148 (2011).
7. A. Ródenas, G. Martin, B. Arezki, N. Psaila, G. Jose, A. Jha, L. Labadie, P. Kern, A. Kar, and R. Thomson, "Three-dimensional mid-infrared photonic circuits in chalcogenide glass," Opt. Lett. **37**(3), 392 (2012).
8. E. M. Purcell, "Spontaneous emission probabilities at radio frequencies," Phys. Rev. **69**(681), 839 (1946).
9. J. L. Jewell, S. L. McCall, Y. H. Lee, A. Scherer, A. C. Gossard, and J. H. English, "Lasing characteristics of GaAs microresonators," Appl. Phys. Lett. **54**(15), 1400–1402 (1989).
10. N. Hodgson and H. Weber, in *Laser Resonators and Beam Propagation-Fundamentals, Advanced Concepts and Applications, Springer Series in Optical Sciences* (Springer, 2005), 108, pp. 189–215.
11. A. Chiasera, R. Belli, S. N. B. Bhaktha, A. Chiappini, M. Ferrari, Y. Jestin, E. Moser, G. C. Righini, and C. Tosello, "High quality factor Er^{3+}-activated dielectric microcavity fabricated by rf sputtering," Appl. Phys. Lett. **89**(17), 171910 (2006).
12. A. Chiasera, F. Scotognella, S. Valligatla, S. Varas, J. Jasieniak, L. Criante, A. Lukowiak, D. Ristic, R. R. Gonçalves, S. Taccheo, M. Ivanda, G. C. Righini, R. Ramponi, A. Martucci, and M. Ferrari, "Glass-based 1-D dielectric microcavities," Opt. Mater. **61**, 11–14 (2016).
13. S. Zamek, L. Feng, M. Khajavikhan, D. T. H. Tan, M. Ayache, and Y. Fainman, "Micro-resonator with metallic mirrors coupled to a bus waveguide," Opt. Express **19**(3), 2417 (2011).
14. W. Bogaerts, P. De Heyn, T. Van Vaerenbergh, K. De Vos, S. Kumar Selvaraja, T. Claes, P. Dumon, P. Bienstman, D. Van Thourhout, and R. Baets, "Silicon microring resonators," Laser Photonics Rev. **6**(1), 47–73 (2012).
15. A. Chiasera, J. Jasieniak, S. Normani, S. Valligatla, A. Lukowiak, S. Taccheo, D. N. Rao, G. C. Righini, M. Marciniak, A. Martucci, and M. Ferrari, "Hybrid 1-D dielectric microcavity: Fabrication and spectroscopic assessment of glass-based sub-wavelength structures," Ceram. Int. **41**(6), 7429–7433 (2015).
16. V. Nazabal, M. Cathelinaud, W. Shen, P. Nemec, F. Charpentier, H. Lhermite, M.-L. Anne, J. Capoulade, F. Grasset, A. Moreac, S. Inoue, M. Frumar, J.-L. Adam, M. Lequime, and C. Amra, "Chalcogenide coatings of Ge15Sb20S65 and Te20As30Se50," Appl. Opt. **47**(13), C114 (2008).
17. M. Sinobad, A. Della Torre, B. Luther-Davis, P. Ma, S. Madden, S. Debbarma, K. Vu, D. J. Moss, A. Mitchell, J.-M. Hartmann, J.-M. Fedeli, C. Monat, and C. Grillet, "Dispersion trimming for mid-infrared supercontinuum generation in a hybrid chalcogenide/silicon-germanium waveguide," J. Opt. Soc. Am. B **36**(2), A98–A104 (2019).
18. E. Delcourt, J. Nessim, L. Bodiou, M. Baillieul, E. Baudet, J. Lemaitre, V. Nazabal, Y. Dumeige, and J. Charrier, "Self-phase modulation and four-wave mixing in a chalcogenide ridge waveguide," Opt. Mater. Express **10**(6), 1440–1450 (2020).
19. T. Kuriakose, E. Baudet, T. Halenkovič, M. M. R. Elsawy, P. Němec, V. Nazabal, G. Renversez, and M. Chauvet, "Measurement of ultrafast optical Kerr effect of Ge–Sb–Se chalcogenide slab waveguides by the beam self-trapping technique," Opt. Commun. **403**, 352–357 (2017).
20. A. Saliminia, A. Villeneuve, T. V. Galstyan, S. LaRochelle, and K. Richardson, "Fabrication of Bragg gratings in multilayer planar waveguide of chalcogenide glasses," in *Technical Digest. Summaries of Papers Presented at the Conference on Lasers and Electro-Optics. Postconference Edition. CLEO '99. Conference on Lasers and Electro-Optics* (IEEE Cat. No.99CH37013) (Opt. Soc. America, 1999), p. 499.
21. S. Ramachandran and S. G. Bishop, "Excitation of Er^{3+} emission by host glass absorption in sputtered films of Er-doped Ge10As40Se25S25 glass," Appl. Phys. Lett. **73**(22), 3196–3198 (1998).
22. T. Halenkovič, J. Gutwirth, P. Němec, E. Baudet, M. Specht, Y. Gueguen, J.-C. Sangleboeuf, and V. Nazabal, "Amorphous Ge-Sb-Se thin films fabricated by co-sputtering: Properties and photosensitivity," J. Am. Ceram. Soc. **101**(7), 2877–2887 (2018).
23. K. Tanaka, "Photo-induced phenomena in chalcogenide glasses," in *Chalcogenide Glasses - Preparation, Properties and Applications* (Woodhead Publishing, 2014), pp. 139–168.

Optical Materials EXPRESS

24. K. Tanaka and K. Shimakawa, *Amorphous Chalcogenide Semiconductors and Related Materials* (Springer, 2011).
25. G. Yang, H. Jain, A. Ganjoo, D. Zhao, Y. Xu, H. Zeng, and G. Chen, "A photo-stable chalcogenide glass," Opt. Express **16**(14), 10565 (2008).
26. W. D. Shen, M. Cathelinaud, M. D. Lequime, F. Charpentier, and V. Nazabal, "Light trimming of a narrow bandpass filter based on a photosensitive chalcogenide spacer," Opt. Express **16**(1), 373 (2008).
27. W. Shen, M. Cathelinaud, M. Lequime, V. Nazabal, and X. Liu, "Photosensitive post tuning of chalcogenide Te20As30Se50 narrow bandpass filters," Opt. Commun. **281**(14), 3726–3731 (2008).
28. P. Němec, J. Charrier, M. Cathelinaud, M. M. B. Allix, J.-L. Adam, S. Zhang, and V. Nazabal, "Pulsed laser deposited amorphous chalcogenide and alumino-silicate thin films and their multilayered structures for photonic applications," Thin Solid Films **539**, 226–232 (2013).
29. K. J. Vahala, "Optical microcavities," Nature **424**(6950), 839–846 (2003).
30. V. Nazabal, F. Starecki, J.-L. Doualan, P. Němec, P. Camy, H. Lhermite, L. Bodiou, M. L. Anne, J. Charrier, and J. L. Adam, "Luminescence at 2.8 μm: Er^{3+}-doped chalcogenide micro-waveguide," Opt. Mater. **58**, 390–397 (2016).
31. S. Normani, G. Louvet, E. Baudet, M. Bouška, J. Gutwirth, F. Starecki, J.-L. Doualan, Y. Ledemi, Y. Messaddeq, J.-L. Adam, P. Němec, and V. Nazabal, "Comparative study of Er^{3+}-doped Ga-Ge-Sb-S thin films fabricated by sputtering and pulsed laser deposition," Sci. Rep. **10**, 7997 (2020).
32. C. J. R. Sheppard, "Approximate calculation of the reflection coefficient from a stratified medium," Pure Appl. Opt. **4**(5), 665–669 (1995).
33. Z.-Y. Li, "Principles of the plane-wave transfer-matrix method for photonic crystals," Sci. Technol. Adv. Mater. **6**(7), 837–841 (2005).
34. D. E. McCumber, "Einstein relations connecting broadband emission and absorption spectra," Phys. Rev. **136**(4A), A954–A957 (1964).